Gap-dependent coupling of Ag-Au nanoparticle heterodimers using DNA origami-based self-assembly

Lee Weller[‡1], *Vivek V. Thacker*[‡1], *Lars O. Herrmann*[1§], *Elisa A. Hemmig*[1], *Anna Lombardi*[1], *Ulrich F. Keyser*[*1], *and Jeremy J. Baumberg*[*1]

[1]Cavendish Laboratory, University of Cambridge, Cambridge, CB3 0HE, UK.

KEYWORDS: DNA origami, plasmonic heterodimers, hybridization, self-assembly

ABSTRACT: We fabricate hetero-component ‘dimers’ built from a single 40 nm gold and a single 40 nm silver nanoparticle separated by sub-5 nm gaps. Successful assembly mediated by a specialized DNA origami platform is verified by scanning electron microscopy and energy-dispersive X-ray characterization. Dark-field optical scattering on individual dimers is consistent with computational simulations. Direct plasmonic coupling between each nanoparticle is observed in both experiment and theory *only* for these small gap sizes, as it requires the silver dipolar mode energy to drop below the energy of the gold interband transitions. A new interparticle-spacing-dependent coupling model for heterodimers is thus required. Such Janus-like nanoparticle constructs available from DNA-mediated assembly provide an effective tool for controlling symmetry breaking in collective plasmon modes.

The reliable fabrication of intricate nanoparticle (NP) geometries by DNA allows for previously impractical characterization of light-matter interactions at the nanoscale. Although the plasmonic properties of *asymmetric* nanostructures have elicited a great deal of interest,(1) most work so far has focused on studies of compositionally homo-component NPs. In the overwhelming majority of studies, identical gold NPs have been used due to their higher chemical stability. Asymmetries can be either due to chemical composition, shape, or size. Interference between the resonances of the individual components in such structures can lead to an overall asymmetric scattering response known as a Fano resonance,(2) seen in a range of structures fabricated with top-down (1) and self-assembly lithography techniques.(3–5)

From a theoretical perspective there are compelling reasons to examine the ideal prototype system built from a dimer consisting of a single Au NP and a single Ag NP.(6,7) The localized surface plasmon resonances (LSPRs) of individual Ag NPs and individual Au NPs are sufficiently separated spectrally that coupling of the 'discrete' Ag plasmon with Au interband transitions (the 'continuum' level) can occur. This should generate an asymmetry in the Ag scattering response which can be further enhanced by using NPs of different sizes.(8) Experimentally, dimers of Au NPs and Au nanoshells have been reported using chemical deposition techniques(3,9) as well 'fanoshells' consisting of a SiO_2 and Au shell layer surrounding a solid Au NP.(4) In 2013, Lombardi *et al.*(5) demonstrated the fabrication of heterodimers formed from Au NPs bound to a core-shell Ag-SiO_2 NP, which include thick SiO_2 spacers that limits the strength of plasmonic coupling. However, *ultra-small gaps* are hard to fabricate with these techniques.

In recent years, self-assembly of DNA nanostructures using the origami technique has emerged as a powerful tool for nanofabrication.(10–12) In particular, DNA origami nanostructures have proved to be reliable platforms for the fabrication of precise geometries of NPs,(13,14) quantum dots(15) and organic dyes(16,17) to study light-matter interactions at the nanoscale. Much attention has focused on the emergence of chirality through the collective

behavior of small (<20 nm) NPs attached to DNA origami platforms.(18–20) Recently, DNA origami nanostructures have also been used to assemble NP architectures from larger (40 nm or greater) NPs.(21–24) These have been custom-designed to ensure stronger plasmonic coupling due to the larger NP size as well as smaller gaps between the NPs. The strength of this plasmonic coupling has been verified and characterized by dark-field scattering.(21) This has enabled the use of such structures for single molecule spectroscopic techniques such as surface enhanced fluorescence(24) and surface enhanced Raman scattering (SERS).(21–23)

In principle, DNA-based self-assembly provides an ideal tool for fabrication of *heterodimer* structures. Although semi-rigid double-stranded (dsDNA) linkers have been used extensively to form homodimers,(25,26) heterodimers,(27) and larger assemblies,(28, 29) the use of such dsDNA linkers on their own introduces variability in the inter-NP spacing(30) compared to rigidity of DNA origami, particularly when they are immobilized and dried on substrates. It is also difficult to fabricate more complex NP geometries using only DNA linkers. Although DNA origami structures have been used for assembling Ag and Au NP geometries,(31) the resulting plasmonic properties (which are exquisitely sensitive to the final geometry) of these structures were not investigated. Similarly, other studies have reported the use of DNA origami templates for top-down fabrication of silver nanoclusters as well as other custom nanoshapes (32,33) but do not characterize the optical properties in detail.

In this paper, we bring together these different ideas and demonstrate the use of DNA origami for the fabrication of compositionally asymmetric heterodimers consisting of one 40 nm Ag NP separated from one 40 nm Au NP by a sub-5 nm gap. A schematic of the structure is shown in Figure 1a (top). This is achieved through the use of a DNA origami platform similar to that reported earlier for Au-Au dimers.(21) Agarose gel electrophoresis is used to separate correctly assembled nanostructures from excess ssDNA-coated NPs and also serves as a verification of correct assembly (Figure 1b). The heterodimers are extracted from the band indicated on the

gel and immobilized on glass substrates for dark-field scattering or Si substrates for scanning electron microscopy (SEM) / energy-dispersive X-ray (EDX) measurements.

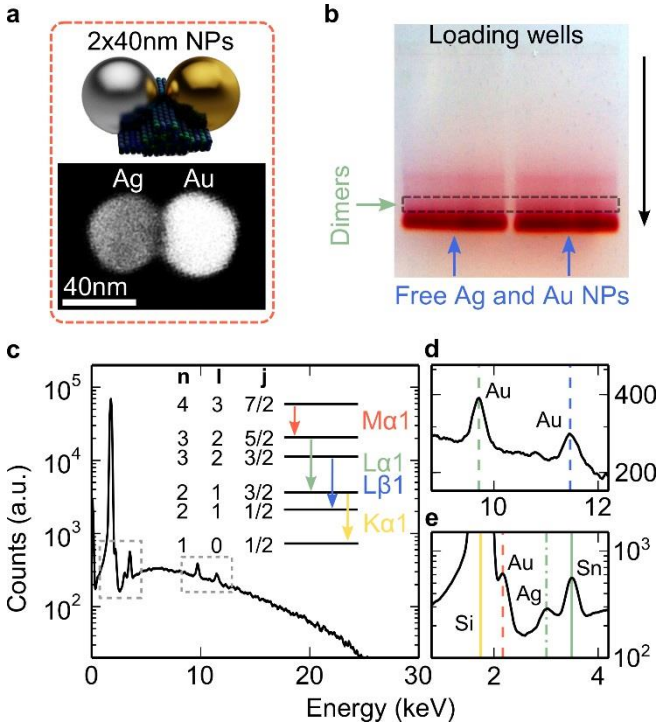

Figure 1: Fabrication and characterization of Ag-Au heterodimers. (a) Schematic (top) and SEM image (bottom) of an individual Ag-Au heterodimer (backscatter contrast). (b) Correctly assembled dimers (in two duplicate runs) are identified as a faint band that runs slower than free ssDNA-coated Au and Ag NPs in a 0.7% agarose gel. (c-e) Heterodimers are characterized using EDX that reveals three characteristic peaks of Au (11.44 keV, 9.71 keV, 2.12 keV), one Ag peak (2.98 keV) and peaks from Si and Sn (**n**, **l,** and **j** correspond to the principal, azimuthal, and total angular momentum quantum numbers respectively).

Further verification of successful assembly is obtained through compositional analysis and elemental mapping using a combined SEM and EDX system. The SEM image of a typical NP dimer (Figure 1a, bottom) clearly reveals the successful formation while the differential contrast is an indicator of the difference in composition between the two NPs. This is further evidenced by EDX measurements which reveal separate signatures of both Au and Ag from the individual nanostructures. As shown in Figure 1c, for a single heterodimer we measure six peaks on top of the continuous background X-rays due to Bremsstrahlung. Assigning these based on Deslattes *et al.*(34) gives three peaks (11.44 keV, 9.71 keV, and 2.12 keV) corresponding to the Lβ1 ($3^2d_{3/2} \rightarrow 2^2p_{1/2}$), Lα1 ($3^2d_{5/2} \rightarrow 2^2p_{3/2}$) and Mα1 ($4^2f_{7/2} \rightarrow 3^2d_{5/2}$) X-ray transitions of Au and one peak (2.98 keV) corresponding to the Lα1 transition of Ag (Figure

1d and 1e). Two additional peaks in Figure 1e (3.44 keV and 1.74 keV) correspond to the Kα1 ($2^2p_{3/2} \rightarrow 1^2s_{1/2}$) and Lα1 transitions of Si (since the samples are immobilized on a Si substrate) and Sn respectively. This additional Sn peak is likely related to impurities (Figure S1). Such elemental mapping shows the darker sphere in Figure 1a is a Ag NP while the brighter sphere is a Au NP of similar size.

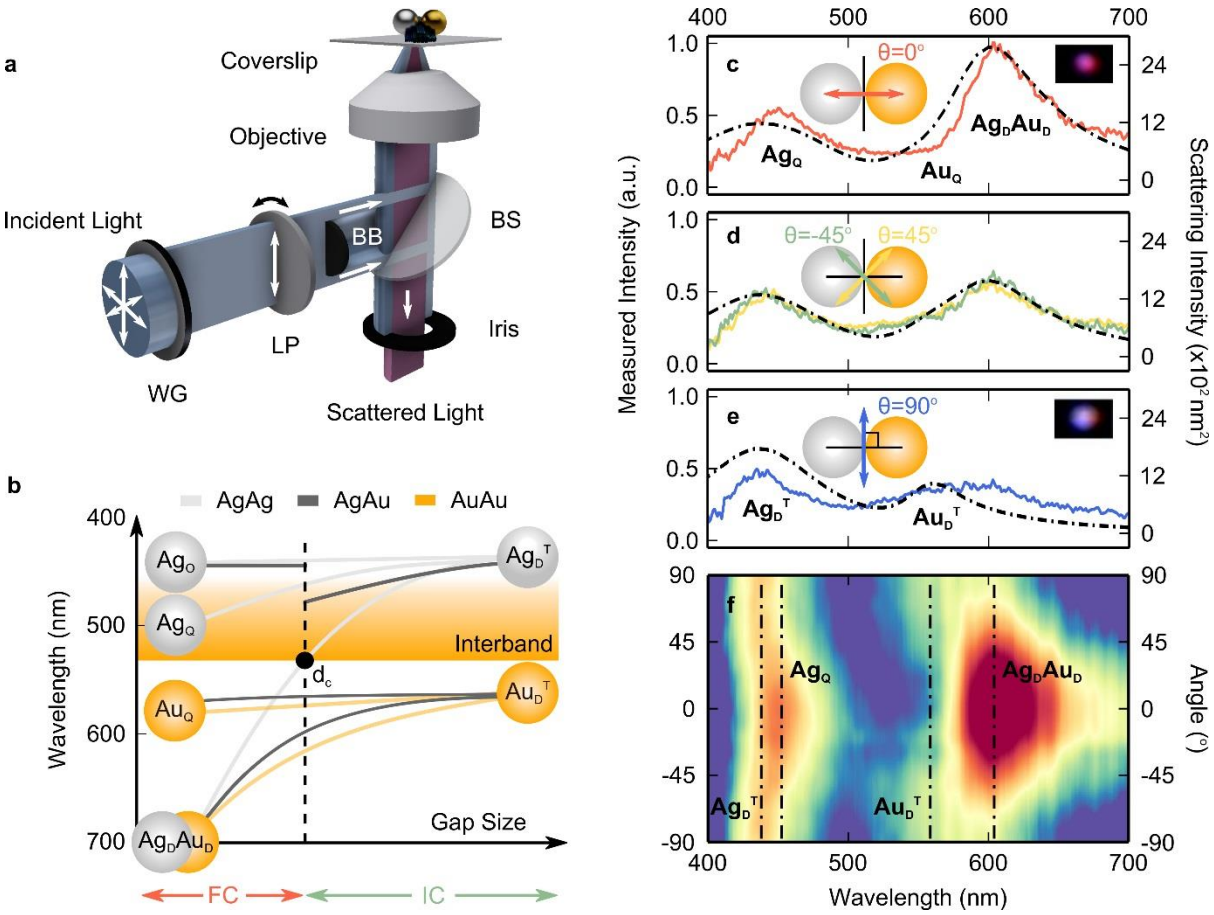

Figure 2: Polarization-dependent dark-field scattering from individual heterodimers. (a) Schematic of the custom-built setup for dark-field scattering from single heterodimer structures with incident white spectrum from 380-900 nm. WG: Wire Grid Polarizer, LP: Linear Polarizer, BB: Beam Block and BS: Beam Splitter. (b) Overview of different modes observed for Ag-Au heterodimers and Au-Au and Ag-Ag homodimers as a function of gap size for longitudinal polarization. The modes are classified according to the electric field distributions around each NP. D: Dipole, Q: Quadrupole, O: Octupole mode. For heterodimers, the critical gap size d_c separates interband coupling (IC) and free coupling (FC) regimes. Modes also observed under transverse polarization (T) are denoted accordingly. Shaded region above 530 nm represents the Au interband continuum. (c-e) Dark-field scattering from a single heterodimer for incident light polarized parallel to the dimer axis (0°), ±45°, and perpendicular to the dimer axis (90°), which agree with predictions from FDTD simulations (dot-dashed lines). Inset images depict the characteristic colors for 0° and 90° polarizations. (f) Color map of the polarization-dependent scattering response of the same heterodimer, spectra taken at intervals of 5°.

Having demonstrated the formation of Ag-Au heterodimers, we characterize their polarization-dependent scattering response and study signatures of coupling between the Ag and Au NPs. The experimental setup is described in Materials and Methods and allows for illumination down to λ=380 nm to enable us to study the optical response of the Ag components (Figure 2a). By rotating the polarization of the incident light, we can characterize the polarization-dependent optical response of individual heterodimers. All polarization artifacts are found to be suitably eliminated in this scheme. Such polarization spectroscopy allows us to uniquely identify dimers in the dark field images, and exclude all stray individual nanoparticles and clusters. In what follows, the angle θ=0° refers to incident light polarized parallel (longitudinal polarization) to the dimer axis while θ=90° refers to incident light polarized perpendicular (transverse polarization) to the dimer axis. Dark-field scattering from a single heterodimer structure is shown in Figure 2c-e, (data for individual Ag and Au NPs is shown in Figure S3). For both θ=0° and θ=90° we observe two peaks in the scattering spectra.

There is disagreement in the literature as to origin of the higher energy mode for each polarization.(7,27) They have previously been attributed to the anti-bonding dipole-dipole modes from a plasmon hybridization model(35) modified by the effect of interband coupling to the Au band structure. Chen *et al.*,(7) instead identifies these as higher-order bonding modes, arguing that the anti-bonding modes are experimentally inaccessible in the UV. We believe that this latter picture is partially right but that a correct description of the nature of these modes is crucially dependent on the interparticle spacing. For gap sizes above a critical distance d_c, there is no overlap between the Ag and Au dipole modes due to interband coupling (IC) with the Au transitions which screens all interactions. Below d_c, free coupling (FC) of the bonding dipole-dipole mode red-shifts the Au dipole mode, but not the quadrupolar modes, while no antibonding dipole-dipole mode is seen in either simulations or experiment even though the heterodimer breaks symmetry. We will investigate the nature of these modes in greater detail below (Figures 3 and 4). We therefore propose a new classification system shown in Figure 2b

that accounts for the modes through dipolar (D), quadrupolar (Q) and octupolar (O) distributions around each single NP within the heterodimer. We find that for the ultra-small gap sizes accessible through our fabrication technique which reach well below a critical gap size ($d_C \sim 8\text{nm}$, see supplementary equation B5), the directly coupled plasmonic dipole-dipole mode can be seen and measured. Modes are labelled therefore with subscripts that describe the predominant *electric field* localization around the Ag NP, the Au NP or both. Transverse modes are additionally indicated by a superscript (T). Hence for instance, Ag_DAu_D is a bonding dipole-dipole mode with the optical field concentrated in the gap between the nanoparticles whereas for the Ag_Q mode, the optical field is predominantly localized in a quadrupole-like symmetry around the Ag NP.

For the particular heterodimer in Figure 2c, at θ=0° we observe a higher-order Ag_Q peak at 449 nm and a bonding dipole-dipole Ag_DAu_D peak at 602 nm. The heterodimer appears pink in color, as shown in the inset image in Figure 2c. As the polarization is rotated towards θ=±45°, the intensity of the Ag_DAu_D peak decreases. The scattering spectra for θ=45° and θ=−45° (Figure 2d) are identical which clearly indicates the dominant bi-axial symmetry of the NP system. At θ=90°, we observe the $Ag_D{}^T$ peak at 435 nm and a broad $Au_D{}^T$ peak around 556 nm (note a small Ag_DAu_D component also remains in the spectra).(36,37) The heterodimer now appears blue in color (Figure 2e, inset), due to the predominant contribution from the $Ag_D{}^T$ peak.

We perform finite-difference time-domain (FDTD) simulations for the NP geometry as described in Materials and Methods. In all the simulations, the surface of the Ag NP is assumed to be covered with a 1 nm thick layer of silver oxide (Ag_2O) to account for the typical oxidation during the dimer fabrication process (which agrees with our simulations, Figure S4), consistent with previous studies for such systems.(38) For each polarization in Figures 2c-e, the experimental data for this particular heterodimer structure agree with predictions from FDTD

simulations (dashed lines) both in intensity and peak position for an inter-particle spacing of 4 nm, which is within the design parameters of the DNA origami platform (mean inter-particle spacing 3.3 ± 1.0 nm) and agrees with our previous work.(21) We clearly observe that the Ag_Q peak is red-shifted by 14 nm from the $Ag_D{}^T$ peak, which is more evident in a detailed map of the polarization-dependent scattering response of this dimer (Figure 2f). The magnitude of the red-shift is dependent upon the interaction with the Au interband continuum (and thus apparently the Fano interaction) in a gap-size dependent manner. At large gap sizes, the Ag_Q peak emerges at the same energy as the $Ag_D{}^T$ peak (Figure S5, S6). On the other hand, for this particular heterodimer with an inter-particle spacing of 4 nm, the corresponding Au_Q mode (indicated in the new classification system in Figure 2b) is weak and difficult to observe.

Previous reports of Ag-Au NP dimers used either thick SiO_2 spacers ($R/d \sim 1$ for gap d and radius R),(5) or double-stranded DNA ($R/d \sim 2$),(27) with correspondingly smaller red-shifts of the Ag_D and Au_D modes than here. In particular the Ag_D mode was never red-shifted to wavelengths longer than the Au interband transitions, so could never directly couple to the free electrons in the Au. For $R/d > 3$ the Ag_D red-shifts beyond the Au interband transitions and a direct plasmonic interaction between the dipoles is possible. Although the Ag and Au NPs used in previous work were always of different sizes to enhance the asymmetry in scattering response, the results shown in Figure 2 demonstrate that consistent sub-5 nm gaps ($<d_C$) offered by our DNA origami platform ($R/d > 4$) allow us to probe this interaction between NPs of the same size.

We study the scattering response of >100 individual heterodimers illuminated near θ=0° in greater detail to explore variations in both gap size and NP diameter. The averaged scattering response is in very good agreement with the FDTD simulations for the designed mean inter-particle spacing of 3.3 nm of the DNA origami platform(21) (Figure 3a). Both the experimental data and simulations clearly show the presence of the weak Au_Q peak at 556 nm. We therefore

perform further FDTD simulations to understand the nature of the Ag-Au interaction in longitudinal polarization for a range of gap sizes (Figure 3b), from 20 nm down to 1 nm. By contrast, similar results for the transverse polarization (Figure S5) show no significant change in peak positions or intensities throughout this range.

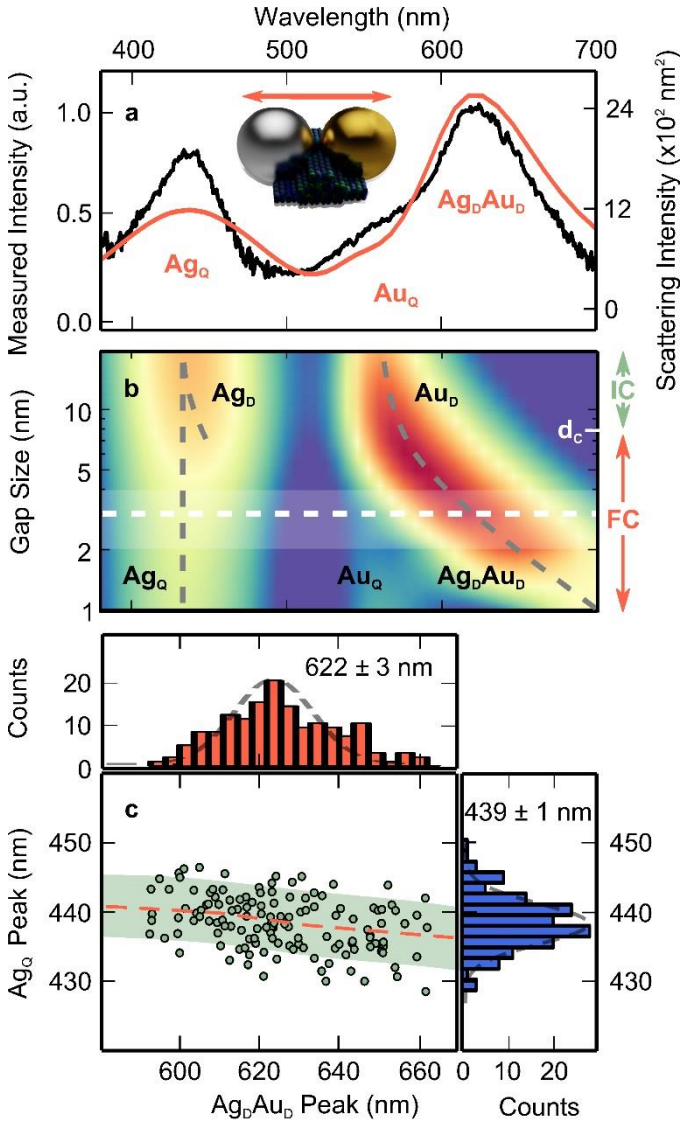

Figure 3: Experimental data and FDTD simulations of Ag-Au coupling. (a) Averaged scattering response of >100 individual heterodimers under longitudinal polarization, which is in good agreement with FDTD simulations. (b) Color map for FDTD simulations of the scattering response as a function of gap size for longitudinal polarization. Mean (standard deviation) inter-particle spacing is indicated by white dashed line (white shaded region). Above and below the critical gap size ($\boldsymbol{d_c}$) are the interband coupling (IC) and free coupling (FC) regimes. (c) Histograms for experimental Ag_Q and Ag_DAu_D spectral peaks. The Ag_Q spectral peak negatively correlates with the Ag_DAu_D peak, in agreement with FDTD predictions (dashed line). Shaded region shows width (FWHM) of the histogram of Ag_Q mode peak positions from >100 individual heterodimers.

A comparison with Au-Au and Ag-Ag homodimers (Figure S6) shows that the Ag-Au interaction in the heterodimer introduces new effects. For large gap sizes (Figure 3b, S7), the high energy mode is predominantly Ag_D (with some small mixing in of higher order modes) and the low energy mode is predominantly Au_D. As with homodimers, both modes red-shift as the gap size decreases. For gap sizes below d_C, three trends are seen: (1) the highest energy Ag_D mode ceases to red-shift and a Ag_Q mode emerges, (2) a weak Au_Q mode emerges, and (3) the lowest energy Au_D mode red-shifts and evolves into the coupled Ag_DAu_D with decreasing gap size.

The emergence of the Au_Q mode is evident in the averaged spectrum in Figure 3a. The surprising behavior of the Ag_Q mode can also be verified experimentally with our heterodimer constructs. The DNA origami platform is designed for a mean inter-particle spacing of 3.3±1.0 nm(21) (indicated by white dashed line and shaded region in Figures 3b), the variation occurring due to the use of dsDNA linkers to tether the NPs to the DNA origami platform. We therefore examined the correlation(39) of the peak positions of the Ag_Q and Ag_DAu_D modes using data from each of the >100 heterodimer structures imaged. The Au_Q and Ag_DAu_D mode peak positions are approximately Gaussian distributed with mean wavelengths at 439±1 nm and 622±3 nm respectively (histograms Figure 3c). The scatter plot in Figure 3c shows that the Ag_Q peak position is indeed *negatively correlated* with Ag_DAu_D peak position as predicted in Figure 3b, and matching the red dashed line from FDTD predictions in Figure 3c.

We have thus uncovered two effects of Ag-Au coupling in such heterodimer structures for sub-5 nm gaps that are verified experimentally and through simulations: the emergence of Au_Q and Ag_Q modes as the gap size decreases below d_C. To understand the nature of the modes for even smaller gap sizes (where the effects are most significant but are not yet experimentally accessible), we perform further FDTD simulations for the optical **E** field intensity (Figure 4a,c,e) and surface charge density distribution (Figure 4b,d,f) for a gap size of 1 nm. We note

how the ultra-small spacing compresses the plasmonic charge distributions around each nanoparticle into the gap region, modifying the underlying symmetries. Instead of being spread evenly around each NP, the lobes of the quadrupolar distributions shrink into the gaps, mixing with the dipolar distributions. Strikingly however, most of the optical field for the Ag_Q and the Au_Q modes is around *either* the Ag *or* the Au NP respectively, whereas the Ag_DAu_D mode shows strong optical fields around *both* NPs (Figure 4e). Indeed, the theoretical work of Chen *et al.*(7) for 60 nm Ag-Au heterodimers predicted surface charge distributions across both NPs but the E fields are distributed predominantly around one NP. These results have so far been ignored due to the lack of experimental verification, which we now report here. This 'decoupling' arises because the Ag_Q mode cannot create image dipoles in the Au (as the Ag quadrupolar mode energy never drops below the energy of the Au interband transitions), just as the dipolar Ag_D mode cannot create image dipoles in the Au when $d>d_C$.

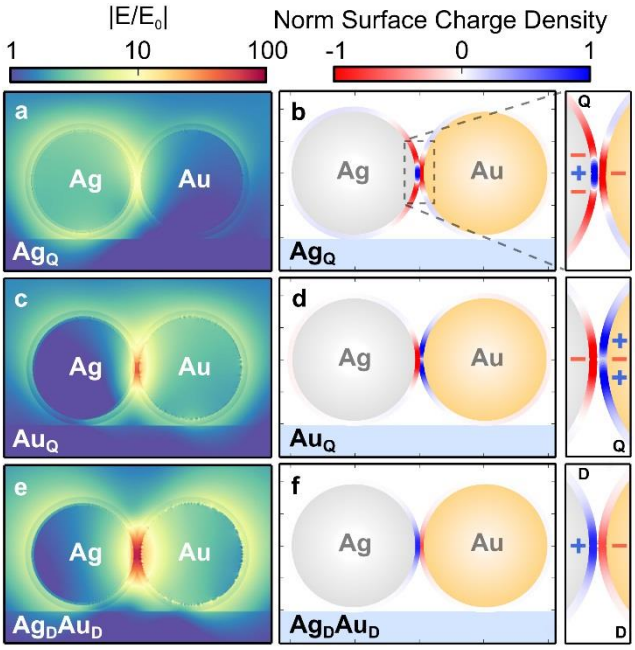

Figure 4: E field and charge distribution for Ag-Au heterodimers. FDTD simulations reveal the **E** field intensities and charge density distributions for the (a, b) Ag_Q, (c, d) Au_Q, and (e, f) Ag_DAu_D modes, for a gap size of 1 nm.

In conclusion, we present here the successful assembly of Ag-Au heterodimers using DNA origami platforms. The polarization-dependent response of such structures is characterized in

detail and found to be consistent with their broken symmetry and hetero-component nature. Importantly, the sub-5 nm gaps provided by the DNA origami platform allowed us to probe the interaction between Ag and Au NPs of the same size which accesses direct dipolar coupling of the Ag and Au electrons. We observe three modes for longitudinal polarization and show their properties match FDTD simulations. A previously-unreported emergence of the Au_Q mode is seen, which we verify with measurements across >100 individual heterodimer structures. These results demonstrate the power of the DNA origami technique to fabricate NP geometries that probe novel interactions between hetero-component structures, and in particular here in an 'apparent free electron coupling regime' which localizes light around either NP. This work holds significant potential for experimental studies in sophisticated complex geometries involving metals, semiconductors, and dielectrics.

DNA origami structure design and assembly

The DNA origami platform design used is identical in dimensions to the one used for the Au-Au NP dimer assembly as reported earlier.(21) The single-stranded DNA (ssDNA) overhangs in the other groove are retained at *t ttt ttt ttt ttt ttt ttt* (complementary to the 'sequence 1' coating on the Au NPs). The sequences of the ssDNA overhangs within one of the grooves were altered to *atg tag gtg gta gag g* (complementary to 'sequence 2' ssDNA coating on the Ag NPs). All short ssDNA staples were purchased from Integrated DNA Technologies. The assembled structures were purified from the excess staple strands by centrifugation with 100 kDa MWCO filters (Amicon Ultra, Millipore) also as described earlier.(21)

ssDNA coating of NPs and synthesis of dimer structures

The protocol used was based on one reported earlier(18,21) but with significant modifications as described below. We use highly concentrated solutions of the NPs as starting materials. Au NPs are obtained from BBI Solutions, UK (optical density (OD) =100) and Ag NPs are obtained from Nanocomposix Inc, USA (BioPure, 1 mg/ml, citrate stabilized). DNA oligos corresponding to ‘sequence 1' or ‘sequence 2' are ordered with a 5' dithiol modification (Biomers.net, Germany). After incubation with 10 mM Tris (2-carboxyethyl) phosphine (TCEP, Sigma Aldrich) for 30 minutes, they are added in a 20000 fold excess to the NP solution.

Next, a sodium citrate-HCl buffer (pH=3) is added to a final concentration of 10 mM and NaCl is added to a final concentration of 30 mM. The NP solutions are then sonicated in a water bath for 15 minutes. This has been reported earlier to increase ssDNA coating efficiency.(40) Finally, HEPES buffer (pH=7) is added at a final concentration of 100 mM. This is then left overnight to further increase the coating efficiency. Successful attachment is confirmed by a lack of aggregation when resuspended in ~50 mM $MgCl_2$.

ssDNA-coated NPs are separated from excess DNA oligos by three rounds of centrifugation with 100 kDa MWCO filters (Amicon Ultra, Millipore) either at 10,000g for 10 minutes (Au NPs) or at 6,000g for 8 minutes (Ag NPs) at 4°C. The fewer rounds of centrifugation also help to maintain the ssDNA coating on the NPs. To account for the fact that there may be a higher proportion of unbound ssDNA in the solution, the filtered NPs are incubated overnight with the assembled DNA origami platforms in 5x excess per binding site. Efforts are also made to ensure that that the concentrations of Au and Ag NPs are roughly similar. Successful formation of dimers and separation from larger aggregates is accomplished by agarose gel electrophoresis in a 0.7% agarose gel run at 50 V and maintained at 4°C by a surrounding ice bath.

We then follow the protocol described earlier(21) to purify the heterodimer structures from the agarose gel and immobilize the assembled nanostructures on glass coverslips, during which

formation of larger aggregates or disassembly of heterodimer structures can occur. Once on the glass coverslip, we estimate that 10% of the structures are heterodimers, with the remainder being either free Au or Ag NPs or larger aggregates. Heterodimers are identified by their polarization-dependent optical response. In addition, every effort is made to use freshly ssDNA coated NPs for assembly, limit the exposure to ambient light during the assembly process, and perform optical studies (dark-field scattering, SEM imaging, EDX measurements) on the immobilized samples as soon as they are prepared to reduce the oxidation of the Ag NPs.

Scattering Spectroscopy

Scattering spectra were measured on a custom built inverted microscopy setup(21,41) suitably modified as follows to allow for illumination down to 380 nm. We employ an incoherent, high-powered, continuous Xenon light source (HPX-2000, 185 – 2000 nm). The polarization of the beam is set using an ultra-broadband wire grid polarizer (WP25M-UB, 250 – 4000 nm) with a greater than 75% transmission and extinction ratio better than 10^3 for the wavelengths of interest (380 – 1000 nm). The polarization angle is rotated with an achromatic half-wave plate (AHWP10M-600, 400 – 800 nm) with a transmission greater than 90% over this region of the spectrum. A beam stop of diameter 4.5 mm then blocks the inner part of the beam, leaving the remaining outer ring for illumination through a bright field objective (Leica HPX Plan APO 63x NA 1.2W) of diameter 6.5 mm. One expects greater than 70% transmission (380 – 1000 nm) with illumination angles of up to 80^o for this objective. The reflected light is then sent through an iris of diameter 4.5 mm allowing only the scattered light from the nanostructure to pass through. Part of the scattered light is collected with a fiber-coupled (50 μm optical fiber) Ocean Optics QE65000 cooled spectrometer. The other fraction is directed towards an Infinity-2 14 bit CCD camera (Lumenera) that allows for wide-field imaging. We use a glass substrate as a reference for the amount of light reflected at each wavelength.

Numerical Simulations

Finite-difference time-domain calculations were carried out with Lumerical FDTD v8.6. Previously,(21) we have shown that the ssDNA layer can be modelled as a 2.5 nm thin dielectric coating (n=1.7) around the Au NP and the DNA origami platform has a refractive index of n=2.1. The combined effect of the ssDNA coating, the DNA origami platform, and the glass coverslips, were implemented as a semi-infinite half-space with a constant real dielectric constant n=1.56, which effectively fits the scattering responses in Figures 2 and 3. Illumination with *s* and *p* polarized plane waves was performed at an angle of incidence of 60° to replicate the lateral and axial polarization components present in the experimental dark-field illumination. The resulting spectra were added incoherently to obtain the scattering cross-section for illumination with unpolarized light.

SEM/EDX measurements

SEM and EDX measurements were taken with a LEO GEMINI 1530VP FEG-SEM, operating at an electron beam energy of 30 keV. The spatial accuracy for the elemental analysis in EDX mode is similar to the resolution of the SEM images.

ASSOCIATED CONTENT

Supporting Information. Figures S1-S7 are available free of charge via the Internet at http://pubs.acs.org.

AUTHOR INFORMATION

Corresponding Author

Email: jjb12@cam.ac.uk and ufk20@cam.ac.uk.

Present address

[§] Photonics Laboratory, ETH Zurich, Honggerbergring 64, 8093 Zurich, Switzerland

Author Contributions

The manuscript was written through contributions of all authors. All authors have given approval to the final version of the manuscript. ‡These authors contributed equally.

ACKNOWLEDGMENTS

We thank Tao Zhang for help with DNA origami platform design. VVT and UFK acknowledge funding from an ERC starting grant Passmembrane 261101. EAH acknowledges funding from Janggen-Pöhn-Stiftung. LW and JJB acknowledge funding from EPSRC EP/G060649/1, EP/K028510/1, and ERC LINASS 320503.

ABBREVIATIONS

REFERENCES

1. Luk'yanchuk, B.; Zheludev, N. I.; Maier, S. A.; Halas, N. J.; Nordlander, P.; Giessen, H. & Chong, C. T. The Fano resonance in plasmonic nanostructures and metamaterials. *Nat. Mater*. **9,** 707–715 (2010).

2. Fano, U. Effects of configuration interaction on intensities and phase shifts. *Phys. Rev.* **124,** 1866–1878 (1961).

3. Brinson, B. E.; Lassiter, J. B.; Levin, C. S.; Bardhan, R.; Mirin, N. & Halas, N. J. Nanoshells made easy: improving Au layer growth on nanoparticle surfaces. *Langmuir* **24,** 14166–14171 (2008).

4. Mukherjee, S.; Sobhani, H.; Lassiter, J. B.; Bardhan, R.; Nordlander, P. & Halas, N. J. Fanoshells: nanoparticles with built-in Fano resonances. *Nano Lett.* **10,** 2694–2701 (2010).

5. Lombardi, A.; Marcin, P. G.; Aurélien, C.; Paolo, M.; Isabel, P.; Luis, M. L.; Natalia, D. & Fabrice, V. Optical response of individual Au-Ag@SiO_2 heterodimers. *ACS Nano* **7,** 2522–2531 (2013).

6. Bachelier, G.; Russier-Antoine, I.; Benichou, E.; Jonin, C.; Del Fatti, N.; Vallée, F. & Brevet, P. F. Fano Profiles Induced by Near-Field Coupling in Heterogeneous Dimers of Gold and Silver Nanoparticles. *Phys. Rev. Lett.* **101,** 197401 (2008).

7. Chen, F.; Alemu, N. & Johnston, R. L. Collective plasmon modes in a compositionally asymmetric nanoparticle dimer. *AIP Adv.* **1,** 032134 (2011).

8. Peña-Rodríguez, O.; Pal, U.; Campoy-Quiles, M.; Rodríguez-Fernández, L.; Garriga, M. & Alonso, M. I. Enhanced Fano Resonance in Asymmetrical Au:Ag Heterodimers. *J. Phys. Chem. C* **115,** 6410–6414 (2011).

9. Brown, L. V.; Sobhani, H.; Lassiter, J. B.; Nordlander, P. & Halas, N. J. Heterodimers: plasmonic properties of mismatched nanoparticle pairs. *ACS Nano* **4,** 819–832 (2010).

10. Rothemund, P. W. K. Folding DNA to create Nanoscale Shapes and Patterns. *Nature* **440,** 297–302 (2006).

11. Douglas, S. M.; Dietz, H.; Liedl, T.; Högberg, B.; Graf, F. & Shih, W. M. Self-assembly of DNA into nanoscale three-dimensional shapes. *Nature* **459,** 414–418 (2009).

12. Dietz, H.; Douglas, S. M. & Shih, W. M. Folding DNA into twisted and curved nanoscale shapes. *Science.* **325,** 725–730 (2009).

13. Ding, B.; Deng, Z.; Yan, H.; Cabrini, S.; Zuckermann, R. N. & Bokor, J. Gold Nanoparticle Self-Similar Chain Structure organized by DNA Origami. *J. Am. Chem. Soc.* **132,** 3248–3249 (2010).

14. Klein, W. P.; Charles, N. S.; Blake, R.; Sadao, T.; William, B. K.; Jeunghoon, L.; Bernard, Y.; William, L. H.; Elton, G. & Wan, K. Multiscaffold DNA Origami Nanoparticle Waveguides. *Nano Lett.* **13,** 3850–3856 (2013).

15. Bui, H.; Craig O.; Carson K.; YerPeng T.; Elton G.; Wan K.; Jeunghoon L.; William B. K.; Bernard Y. & William L. Hughes Programmable Periodicity of Quantum Dot Arrays with DNA origami Nanotubes. *Nano Lett.* **10,** 3367–3372 (2010).

16. Schreiber, R.; Do, J.; Roller, E.; Zhang, T.; Schüller, J. V.; Nickels, C. P.; Feldmann, J. & Liedl, T. Hierarchical assembly of metal nanoparticles, quantum dots and organic dyes using DNA origami scaffolds. *Nat. Nanotechnol.* **9,** 74–78 (2014).

17. Steinhauer, C.; Jungmann, R.; Sobey, T. L.; Simmel, F. C. & Tinnefeld, P. DNA origami as a nanoscopic ruler for super-resolution microscopy. *Angew. Chem. Int. Ed.* **48,** 8870–8873 (2009).

18. Kuzyk, A.; Schreiber, R.; Fan, Z.; Pardatscher, G.; Roller, E.; Högele, A.; Simmel, C. F.; Govorov, O. A. & Liedl, T. DNA-based Self-Assembly of Chiral Plasmonic Nanostructures with Tailored Optical Response. *Nature* **483,** 311–314 (2012).

19. Shen, X.; Song, C.; Wang, J.; Shi, D.; Wang, Z.; Liu, N. & Ding, B. Rolling up Gold Nanoparticle-dressed DNA Origami into Three-Dimensional Plasmonic Chiral Nanostructures. *J. Am. Chem. Soc.* **134,** 146–149 (2012).

20. Shen, X.; Asenjo-Garcia, A.; Liu, Q.; Jiang, Q.; Javier García de Abajo, F.; Liu, N. & Ding, B. Three-Dimensional Plasmonic Chiral Tetramers Assembled by DNA Origami. *Nano Lett.* **13,** 2128–2133 (2013).

21. Thacker, V. V.; Herrmann, L. O.; Sigle, D. O.; Zhang, T.; Liedl, T.; Baumberg, J. J. & Keyser, U. F. DNA origami based assembly of gold nanoparticle dimers for surface-

enhanced Raman scattering. *Nat. Commun.* **5,** 3448 (2014).

22. Kühler, P.; Roller, E. M.; Schreiber, R.; Liedl, T.; Lohmüller, T. & Feldmann, J. Plasmonic DNA-origami nanoantennas for surface-enhanced Raman spectroscopy. *Nano Lett.* **14,** 2914–2919 (2014).

23. Prinz, J.; Schreiber, B.; Olejko, L.; Oertel, J.; Rackwitz, J.; Keller, A. & Bald, I. DNA Origami Substrates for Highly Sensitive Surface-Enhanced Raman Scattering. *J. Phys. Chem. Lett.* **4,** 4140–4145 (2013).

24. Acuna, G. P.; Möller, F. M.; Holzmeister, P.; Beater, S.; Lalkens, B. & Tinnefeld, P. Fluorescence Enhancement at Docking Sites of DNA-Directed Self-Assembled Nanoantennas. *Science.* **338,** 506–510 (2012).

25. Busson, M. P.; Rolly, B.; Stout, B.; Bonod, N.; Larquet, E.; Polman, A. & Bidault, S. Optical and Topological Characterization of Gold Nanoparticle Dimers Linked by a Single DNA Double Strand. *Nano Lett*. **11**, 5060-5065 (2011).

26. Piantanida, L.; Naumenko, D. & Lazzarino, M. Highly efficient gold nanoparticle dimer formation via DNA hybridization. *RSC Adv*. **4**, 15281-15287 (2014).

27. Sheikholeslami, S.; Jun, Y.; Jain, P. K. & Alivisatos, A. P. Coupling of optical resonances in a compositionally asymmetric plasmonic nanoparticle dimer. *Nano Lett.* **10,** 2655–2660 (2010).

28. Jin, R.; Wu, G.; Li, Z.; Mirkin, C. A. & Schatz, G. C. What controls the melting properties of DNA-linked gold nanoparticle assemblies?. *J. Am. Chem. Soc*. **125**, 1643-1654 (2003).

29. Lermusiaux, L.; Maillard, V.; & Bidault, S. Widefield spectral monitoring of nanometer distance changes in DNA-templated plasmonic rulers. A*CS Nano* **9**, 978-990 (2015).

30. Lerch, S.; & Reinhard, B.M. Quantum plasmonics: Optical monitoring of DNA-mediated charge transfer in plasmon rulers. *Adv. Mat.* **28,** 2030-2036 (2016).

31. Pal, S.; Deng, Z.; Ding, B.; Yan, H. & Liu, Y. DNA-origami-directed self-assembly of discrete silver-nanoparticle architectures. *Angew. Chem. Int. Ed.* **49,** 2700–2704 (2010).

32. Copp, S. M.; Schultz, D. E.; Swasey, S. & Gwinn, E. G. Atomically precise arrays of fluorescent silver clusters: a modular approach for metal cluster photonics on DNA nanostructures. *ACS Nano* **9,** 2303–2310 (2015).

33. Shen, B.; Linko, V.; Tapio, K.; Kostiainen, M. A. & Toppari, J. J. Custom-shaped metal nanostructures based on DNA origami silhouettes. *Nanoscale* **7,** 11267–11272 (2015).

34. Deslattes, R. D.; Kessler Jr, G. E.; Indelicato, P.; De Billy, L.; Lindroth, E. & Anton, J. X-ray transition energies: new approach to a comprehensive evaluation. *Rev. Mod. Phys.* **75,** 35–99 (2003).

35. Nordlander, P.; Oubre, C.; Prodan, E.; Li, K. & Stockman, M. I. Plasmon Hybridization

in Nanoparticle Dimers. *Nano Lett.* **4,** 899–903 (2004).

36. Barrow, S. J.; Funston, A. M.; Gómez, D. E.; Davis, T. J. & Mulvaney, P. Surface plasmon resonances in strongly coupled gold nanosphere chains from monomer to hexamer. *Nano Lett.* **11,** 4180–4187 (2011).

37. Brown, K. R.; Walter, D. G. & Natan, M. J. Seeding of Colloidal Au Nanoparticle Solutions. 2. Improved Control of Particle Size and Shape. *Chem. Mater.* **12,** 306–313 (2000).

38. Chatterjee, K.; Banerjee, S. & Chakravorty, D. Plasmon resonance shifts in oxide-coated silver nanoparticles. *Phys. Rev. B.* **66**, 085421 (2002).

39. Hughes, I. G. & Hase, T. P. A. Measurements and Their Uncertainties: A Practical Guide to Modern Error Analysis. *OUP*. (2010).

40. Hurst, S. J.; Lytton-Jean, A. K. R. & Mirkin, C. A. Maximizing DNA loading on a range of gold nanoparticle sizes. *Anal. Chem.* **78,** 8313–8318 (2006).

41. Herrmann, L. O. & Baumberg, J. J. Watching Single Nanoparticles Grow in Real Time through Supercontinuum Spectroscopy. *Small* **9,** 3743-3747 (2013).

42. Benz, F.; De Nijs, B.; Tserkezis, C.; Chikkaraddy, R.; Sigle, D. O.; Pukenas, L.; Evans, S. D.; Aizpurua, J. & Baumberg, J. J. Generalized circuit model for coupled plasmonic systems. *Opt Exp*. **23,** 33255-33269 (2015).

Insert Table of Contents Graphic and Synopsis Here